



# Mixing and segregation of wheat bran and vegetable pieces binary mixtures in fluidized and fluid-spout beds for atmospheric freeze-drying

Mauricio M. Coletto , Daniele L. Marchisio & Antonello A. Barresi

To cite this article: Mauricio M. Coletto , Daniele L. Marchisio & Antonello A. Barresi (2017) Mixing and segregation of wheat bran and vegetable pieces binary mixtures in fluidized and fluid-spout beds for atmospheric freeze-drying, *Drying Technology*, 35:9, 1059-1074, DOI: [10.1080/07373937.2016.1230741](https://doi.org/10.1080/07373937.2016.1230741)

To link to this article: <http://dx.doi.org/10.1080/07373937.2016.1230741>



Accepted author version posted online: 04 Oct 2016.  
Published online: 04 Oct 2016.



[Submit your article to this journal](#)



Article views: 33



[View related articles](#)



[View Crossmark data](#)

## Mixing and segregation of wheat bran and vegetable pieces binary mixtures in fluidized and fluid-spout beds for atmospheric freeze-drying

Mauricio M. Coletto , Daniele L. Marchisio , and Antonello A. Barresi 

Department of Applied Sciences and Technology, Politecnico di Torino, Turin, Italy

### ABSTRACT

The segregation of binary mixtures of nonfood wheat bran and vegetables at different levels of dryness was studied by simulating different stages of the atmospheric freeze-drying by immersion in an adsorbent material process. It was characterized using a new set of four indices, which allow to evaluate not only the segregation level but also the segregation pattern. The mixing performance was evaluated in a fluidized bed (considering also the effect of air superficial velocity) as well as in a spout-fluid bed; peas, carrot disks, and potato slabs were used as food products. In general, it was found that food material segregates toward the bed bottom during the first stages of the drying process in fluidized beds, which translates in a poor contact product-adsorbent. On the contrary, uniform mixing patterns were observed in the spout-fluid bed, for the beginning and final stages of the process. On the other hand, despite the very low cost of nonfood wheat bran and its compatibility with food materials, it presents a channeling fluidization as a consequence of the cohesive properties of its particles. This behavior was also characterized by video analysis in two different fluidized beds. A channel generation and collapse general cycle were highlighted, whose frequency and channel characteristics depend on the air superficial velocity. In addition, three main types of food particle transports were identified: passive (downward), active (upward), and particle-blocking effects. These findings allowed to explain segregation phenomena in these kinds of binary mixtures.

### KEYWORDS

Atmospheric freeze-drying; binary mixtures; cohesive powder; segregation; spout-fluid bed

### Introduction

Binary mixtures occur frequently in the food industry and their complex behavior would make the process difficult in handling, reducing the efficiency of the process, or impacting on the final quality of the product. Atmospheric freeze-drying by immersion in an adsorbent material in a fluidized bed (AFD-IAM-FB) is one of the cases in which food technology faces with technical difficulties.

In general terms, in the lyophilization process (also known as freeze-drying), previously frozen material is dried by ice sublimation at low temperature. Normally, a primary drying stage for removing frozen water is followed by a secondary drying for evaporating the remaining bounded water. Basically, this process can be performed either at atmospheric pressure AFD<sup>[1]</sup> or under vacuum (vacuum freeze-drying, VFD).<sup>[2,3]</sup> In the first case, it is essential that the water partial pressure is maintained at very low values, below ice vapor tension, to allow sublimation, but the freeze-drying might be combined with the application of

microwaves,<sup>[4,5]</sup> ultrasound,<sup>[6,7]</sup> and various other methods to enhance and/or accelerate drying, as it was described in an extensive review by Pisano et al.<sup>[8]</sup>

Atmospheric freeze drying has been getting importance in the last years for industrial food applications, as a consequence of its relatively reduced operating costs and the higher quality of the final products compared with that obtainable with conventional drying. Many authors have been working on this process during last three decades, investigating different factors affecting heat and mass transfer, improving them with some extra energy supply, and/or evaluating final product quality from the point of view of shape, color, or rehydration capacity.<sup>[9–13]</sup> In addition, different types of equipments were also proposed to perform AFD, ranging from tunnel driers or fixed beds to fluidized beds, either standard, vibro, or pulsed.<sup>[14–16]</sup>

Duan et al.<sup>[17]</sup> reviewed recent literature on freeze-drying considering not only the available techniques for freeze-drying, till now, but also the effect of temperature on generated pores during the drying

process and its results on product quality, energy costs, and efficiency, and it also highlighted the main features and process control strategies of microwave-assisted freeze-drying, AFD, and VFD.

In particular, various researchers have investigated the main variables influencing the AFD in fluidized beds. However, this process is usually performed with air at temperatures between  $-15$  and  $-5^{\circ}\text{C}$ , which therefore can reach saturation rapidly. This situation leads to a reduction of the gradient of water concentration between the air and the product surface, and consequently, to a diminution of the mass transfer rate. AFD-IAM may thus be a good technical solution to maintain a low water partial pressure in the air along all the bed. Moreover, the use of the adsorbent medium presents two additional advantages: first, as the heat of adsorption of water vapor is of the same order of magnitude of the sublimation heat of ice, no additional energy supply is necessary; second, it acts as an adsorbent medium for the generated water vapor, allowing to recirculate the drying air, which means an additional reduction of operating costs.

Donsi et al.<sup>[18]</sup> investigated the influence of many factors, such as freeze-drying temperature, fluidization velocity, nature of adsorbent material, size of adsorbent particles, and product/adsorbent weight ratio, on the final drying rate, using different materials as adsorbent and potato disks as products. It was found that the fluidization velocity has no important effect on the drying rates, and at high product concentration, the foodstuff segregates, leading to poor contact with the adsorbent. Further results by Di Matteo<sup>[19]</sup> evidenced that at lower product concentrations, the drying process takes place more rapidly, in other words, the product's absolute humidity ( $\text{kg}_{\text{water}}/\text{kg}_{\text{dry}}$ ) decreases faster. However, product to adsorbent ratios less than 1/20 have no significant effects on augmenting the drying velocity as the processes are controlled by external mass transfer during the first period itself.

Wolff and Gibert<sup>[20]</sup> developed a model for the simulation of AFD processes, under certain assumptions. They performed some experiments that reflected the influence of parameters such as temperature, water content, product to adsorbent mass ratio, shape and size of the product to be dehydrated, and temperature for adsorbent regeneration. They used potato slices as product and starch as adsorbent. Nevertheless, the authors did not mention whether segregation phenomena or formation of channels were present or not.

Due to its compatibility with food products and very low price, since it is a by-product of wheat processing, nonfood wheat bran seems to be a promising material to be used for AFD. Nonetheless, as it is the hard outer

layer of cereals consisting of combined aleurone and pericarp, obtained as a by-product of milling in the production of refined grains, its particles exhibit a very irregular plane shape, with rests of grain brush and, in some cases, broken pericarp. These characteristics confer to the particles a rough surface and, as undesired consequence, the possibility of mechanical interaction during fluidization.

In addition, when AFD-IAM-FB is evaluated, it is important to consider not only the interplay between particles of the adsorbent phase but also the interaction between food pieces and adsorbent. In other words, segregation phenomena should be taken into account in this case, as two particulate systems of completely different size and density are fluidized in the same bed.

According to Rowe et al.<sup>[21]</sup> (who investigated bubbling fluidized beds of noncohesive materials), density differences are the main causes of segregation in gas fluidized beds, whereas size differences have a slight influence when the mixture is made up of particles of equal density and different size. Moreover, working with mixtures composed of solids of different densities, Qiaoquna et al.<sup>[22]</sup> observed that an increment on the mixture mean diameter, by either augmenting the overall mass fraction of the larger particles or using particles with greater diameter for one of the phases, increases the mixture minimum fluidization velocity. This results in a reduction of air excess velocity and, consequently, the segregation of the particulate system is potentiated.

Regarding fluidization time, the minimum elapsed time required to reach segregation equilibrium depends on the excess velocity used and larger to smaller particle diameter ratio. For excess air velocities greater than 0.16 m/s, 20 min were found sufficient to achieve good mixing. Moreover, the same fluidization time is sufficient for diameter ratios up to 4.8.<sup>[23]</sup>

One of the main mixing factors in noncohesive systems are air bubbles, which carry particles in their wakes. The number and size of bubbles might depend on air velocity and particle size distribution (PSD).<sup>[24]</sup> Nonetheless, mixing and segregation in cohesive or pseudo-cohesive systems (which share characteristics of cohesive and noncohesive powders) may be affected by different factors rather than bubbles, such as channel generation and collapse.

To obtain a better understanding of the segregation phenomenon, it is important to study the fluid dynamics of the fluidized beds and the behavior of the components of the mixture during fluidization. Considering the density and Sauter's diameter of the powder particles, its most probable behavior in a fluidized bed can be predicted referring to its Geldart's classification.<sup>[25]</sup>

However, some powders like nonfood wheat bran may be classified into a given category according to their density and diameter, but may behave differently because of their physical characteristics described above. Another important indicator of the dynamics of a fluidized bed are the pressure drop oscillations. They depend on particle properties, bed characteristics, and air velocity and might be related to bubbling, slugging, or turbulent fluidization.<sup>[26]</sup>

In the fluidization of cohesive powders, the interparticle forces are greater than the drag forces leading to the formation of plugs in small diameter fluidized beds and channels in larger ones. These interparticle forces may be caused by either electrostatic charges or liquid bridges (wet or sticky materials).<sup>[25]</sup> In particular, the main cohesive forces between particles in a powder are van der Waals forces, which can be perceived only by very small particles (few microns or less), depending on the particle density, porosity, and surface roughness.<sup>[27]</sup> On the other hand, an increment on the moisture level of the bed results in an increase in the interparticle forces due to liquid bridges, causing a reduction of the bed expansion at low gas velocities but rises at high velocities.<sup>[28]</sup> Moreover, particles may link together in layer/plate structures resulting in a extra frictional forces with the bed walls, increasing the pressure drop during the packed-bed regime.<sup>[29]</sup> Further information and discussions about this pressure overshoot and other factors involved in cohesive fluidization can be found in an exhaustive review paper published by Sundaresan.<sup>[30]</sup> In addition, the cohesive forces can be approached by mathematical models taking into account the formation of agglomerates and effective agglomerate diameter as done by Zhou and Li<sup>[31]</sup> and van Wachem and Sasic.<sup>[32]</sup>

An improvement of the material circulation and solid mixing can be obtained by considering different kinds of beds for AFD-IAM. The “spout-fluid bed” (a modified spouted bed with auxiliary air injectors located in the lower section of the bed) seems to be an interesting example, as it presents better solid mixing and annular solid–fluid contact than standard spouted beds, and better performance when cohesive solids are used.<sup>[33]</sup> Though the particle diameter ratio has a pronounced effect on segregation even for these kinds of beds, particularly for Geldart D glass beads, reducing the mixing degree of the binary mixture as the size difference increases.<sup>[34–36]</sup> On the contrary, particle density differences seem to exert a reduced effect on segregation using high air velocities in the main injector.<sup>[37]</sup>

Additionally, many works can be found in the literature on spout-fluid beds, evaluating their characteristics as drying apparatus,<sup>[38,39]</sup> investigating in particular their hydrodynamics,<sup>[40]</sup> their fluidization regimes,<sup>[41,42]</sup>

developing correlations for predicting fountain height, and discussing modeling aspects.<sup>[43,44]</sup>

Most of the previously mentioned works and other papers found in the literature were performed using noncohesive powders forming binary mixtures whose components had diameters not greater than 1 or 2 mm. Besides, in most of the cases, spherical or nearly spherical particles were utilized in the mixtures. Therefore, there is a lack of information about the behavior of fluidization of binary mixtures of a cohesive or pseudo-cohesive solid and not spherical particles with equivalent diameters in the order of centimeters, and in particular, there is a lack of knowledge about how a pseudo-cohesive powder like nonfood wheat bran works in a fluidized bed or a fluid-spouted bed, its behavior as component of binary mixtures with particles up to two orders of magnitude greater, and the link between channeling and mixing.

Therefore, a deeper study about the characteristics of this very cheap material and its hydrodynamic interactions with food particles should be performed before investigating the AFD of food applying it as adsorbent.

On the other hand, a particular approach to mixing/segregation indices is needed allowing a more precise quantification of the segregation phenomenon and comparison between different beds.

The main objective of the present work is twofold: on one hand to characterize the hydrodynamic behavior of nonfood wheat bran, as potential adsorbent for AFD-IAM in fluidized bed as well as spout-fluid bed; on the other hand to study the segregation of binary mixtures of nonfood wheat bran and vegetables at different levels of dryness simulating the process of drying and to establish the ideal conditions under which AFD-IAM can be performed without excessively reducing the product size.

Fluidized beds will be investigated in detail, but very strong segregation problems will be evidenced in this type of apparatus, while spout-fluid beds appear as the suitable technology for uniform fluidization. Also the segregation mechanisms occurring in this type of beds will be deeply investigated to evidence differences with respect to bubbling fluidized beds.

## Materials and methods

### Food material and adsorbent

Knowing the nonfood wheat bran absolute density ( $1,469 \text{ kg/m}^3$ ) and its minimum fluidization velocity ( $0.17 \text{ m/s}$ ) obtained from preliminary experiments, an equivalent diameter for fluidization (EDF) was estimated by solving the Ergun’s equation for the

particle diameter:

$$0 = \frac{1650u_{mf}\mu}{g} \frac{1}{d_{eq}^2} + \frac{24.5u_{mf}^2\rho_{air}}{g} \frac{1}{d_{eq}} + (\rho_{air} - \rho_A) \quad (1)$$

which was estimated to be 626.6  $\mu\text{m}$ .

Then, according to this information and the absolute density, it was classified as B type in the Geldart's classification of powders.<sup>[25]</sup> Moreover, from image analysis, the bran particle thickness was determined to be around 140  $\mu\text{m}$ .

From sieving analysis and estimation of the Sauter diameter of each class of non-food wheat bran, it comes out that about 90% of particle population belongs to Geldart B group, and only approximately 10% to Geldart A. In other words, the presence of Geldart C (cohesive) particles is negligible.

Fresh food material was purchased in the local market and cut in disks, slabs, or cubes (Table 1). Lyophilized material was obtained by VFD in a small-size industrial apparatus (*LyoBeta 25<sup>TM</sup>* by Telstar, Terrassa, Spain), using the same conditions for every food material.

### Experimental apparatus

According to the characteristics of each experiment series, different fluidized beds were utilized. Table 2 presents the utilized beds, their characteristics, and the experiment types performed in each one. In all the cases, air at ambient temperature was used (about 25°C).

In both L35b (Fig. 1a) and L20b fluidized beds, air is injected into the bed through a gas distributor consisting of a square perforated plate. The hybrid spouted bed (fluid-spout bed) has lateral air injectors situated at the bed bottom added to its central air jet (Fig. 1b), which help to avoid the accumulation of larger material at the bed bottom. In the figure, it is evidenced the position of the distributor screw as it can have an effect on the product quality as it will be discussed in the Results and discussion section.

During preliminary fluidization tests, it was found that the utilized bran fluidizes more like a cohesive powder rather than a Geldart B one. Thus, aiming to obtain a qualitative description and quantitative data about the fluidization behavior of a binary mixture (containing nonfood wheat bran) in the 35-cm-sided fluidized bed, videos were taken while doing fluidization experiments, through its Plexiglas window (camera *Panasonic DMC-TZ4*, video mode, 25 frames/s). Then, they were analyzed frame by frame and information about bed height, number of frontal channels, and the variation of these variables during the fluidization at different velocities was taken. Only the number of frontal channels was considered, as it was quite complicated to measure the total number of channels. However, by visual inspection in the L35b fluidized bed, it was observed that this variable is proportionally representative of the number of channels in the rest of the bed at 1.5 and 1.7 times the adsorbent minimum fluidization velocity ( $u_{mfA}$ ).

Another series of experiments were performed in the geometrically similar L20b fluidized bed using binary mixtures. Also in this case videos were taken through the bed Plexiglas frontal wall for frame by frame analysis. These experiments were done with the scope of obtaining a general idea about the behavior of channel formation and solid phase interaction. Although there would be some differences concerning to channel length or their diameters between the two beds, the main idea was to better observe the channeling phenomenon already seen in the upper part of the 35-cm sided bed.

Furthermore, to obtain better information about the pressure drop during channel generation and collapse of wheat bran, experiments in a small Plexiglas 65 mm diameter cylindrical bed (L065b) were performed, measuring pressure drop using a water manometer. The small diameter of the fluidized bed was particularly chosen because it allows the formation of only one channel with the used wheat bran. Videos were taken in this case as well.

**Table 1.** Utilized food material with its shape characteristics.

Code	Material	Particle shape	Dimensions (mm)	$d_{sv}$ (mm)	$\psi$	$\rho$ (kg/m <sup>3</sup> )
CAf	Fresh carrot	Disc	$l=5.0, d=35.0$	11.7	0.557	$1,050 \pm 55$
CAa	Lyophilized carrot	Disc	$l=5.0, d=18.0$	9.5	0.719	$158 \pm 8$
CAb	Lyophilized carrot	Disc	$l=5.0, d=21.0$	10.2	0.681	$112 \pm 6$
POa	Lyophilized potato	Slab	$l_1=l_2=12.5, l_3=5.0$	8.3	0.729	$176 \pm 11$
POb	Fresh potato1	Cube	$l=10.0$	10.0	0.806	$1,070 \pm 13$
POc	Fresh potato2	Slab	$l_1=l_2=12.5, l_3=5.0$	8.3	0.729	$1,070 \pm 13$
POd	Lyophilized potato	Slab	$l_1=l_2=40.0, l_3=5$	12.0	0.484	$198 \pm 8$
PEa	Lyophilized pea	Sphere	$d=8.8$	8.8	1.000	$202 \pm 7$
PEb	Partially lyophilized pea	Sphere	$d=8.8$	8.8	1.000	$401 \pm 14$
PEc	Lyophilized pea	Sphere	$d=8.8$	8.8	1.000	$237 \pm 8$
PEf	Fresh pea	Sphere	$d=8.8$	8.8	1.000	$1,088 \pm 37$

**Table 2.** Type of fluidized bed used (ID code, characteristics, and experiments done in each one).

ID	Section shape	Base dimensions (mm)	Other characteristics	Experiments done	Pressure probe position
L35b	Square	350 × 350	–	Bran hydrodynamics; segregation and mixing	115 mm from distributor
L20b	Square	200 × 200	–	Bran hydrodynamics	Not used
L065b	Circle	65	Cylindrical	Bran hydrodynamics	5 mm from distributor
L20spjet	Rectangle	200 × 100	Spout-fluid bed	Segregation and mixing	Not used

*Bran hydrodynamics:* Hydrodynamic study of non-food wheat bran alone.

### Mixing and segregation experiments

Different binary mixtures containing bran and lyophilized food materials were utilized to evaluate the effect of particle shape, food concentration, fluidization time, food density, and air velocity on segregation. To eliminate the dependence on the initial mixture state and to highlight the influence of previous parameters, these experiments were mainly performed loading initially homogeneously mixed binary mixtures; but a series of experiment was also performed starting with nonhomogeneously mixed mixtures.

The homogeneous mixtures were previously prepared by equally dividing the total amount of food material and adsorbent in few smaller quantities. They were separately mixed and, finally, gradually loaded one by one into the fluidized bed (in the L035b, through the Plexiglas window when possible or a lateral removable window near the top; in the L020spjet, directly from the top).

Segregation was evaluated by a novel index set, the three-thirds segregation index set (TTSIS), consisting of three numbers that evaluate the distribution profile of a material of interest (food product, for the current case) and a fourth one that gives an idea of the segregation level. The first index is the bottom third indicator, the second one is the middle third indicator, the third one is the top third indicator, and the last one is the segregation level. These indices are, respectively,

labeled as  $p_I$ ,  $p_M$ ,  $p_S$ , and  $N_2$  and together are expressed as  $[p_I, p_M, p_S]_{N_2}$ .

Considering  $h^*$  as the dimensionless position in the bed from the bottom (calculated as the ratio of the height in the bed from the bottom and the total bed height in settled state), and defining  $F_q(h^*)$  the accumulated mass of material of interest “q” as a function of  $h^*$ , these three indicators are calculated as follows:

$$p_I = \frac{F_q(\frac{1}{3})}{m_{qT}} \quad (2)$$

$$p_M = \frac{F_q(\frac{2}{3}) - F_q(\frac{1}{3})}{m_{qT}} \quad (3)$$

$$p_S = \frac{m_{qT} - F_q(\frac{2}{3})}{m_{qT}} \quad (4)$$

and

$$N_2 = \max(p_I, p_M, p_S) - \min(p_I, p_M, p_S) \quad (5)$$

Based on the values obtained with the TTSIS, different segregation patterns can be identified (i.e., full top, uniform, bottom central). Further information on experimental determination of above parameters, about the extreme and intermediate values of TTSIS, and criteria utilized for classification of the segregation patterns can be found in previous works.<sup>[45,46]</sup> Additional details, performance analysis, and comparison with other mixing indices can be found in the cited thesis and article.

To investigate the food particles displacement during the fluidization, some of them were marked as tracers in some experiments. Two kinds of tracers were differentiated with different colors: top tracers (initially in the upper third of the bed) and bottom tracers (initially in the lowest third of the bed). TTSIS was also calculated for tracer particles, allowing an easy and simple description of the foodstuff movements during the process.

Furthermore, experiments in the spout-fluid bed (L20spjet) were performed based on the results of the segregation experiments and the study of bran behavior during fluidization at different velocities. Only one concentration of food material was used (1/20 fresh product to bran mass ratio), and the maximum air velocity that does not cause the transport of bran and food material out of the bed, with 20 min of fluidization time, was applied.

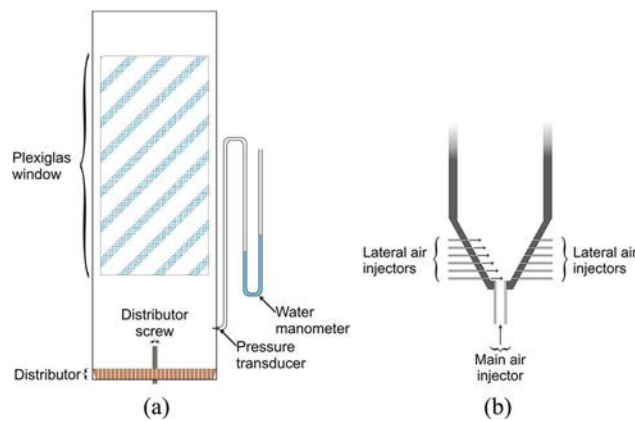


**Figure 1.** Utilized beds. (a) L35b (350-mm-sided fluidized bed). L20b is similar but smaller and its plexiglas window extends to all the bed height. (b) L20spjet (200-mm spout-fluid bed).

### Fluidization time and layer vacuuming

Except for experiments starting with inhomogeneous mixtures or special tests for evaluating the effect of time on segregation, the applied fluidization time was 20 min for experiments performed in the fluidized bed (L35b) as well as in the fluid-spout bed (L20spjet). This fluidization time was particularly chosen based on the work of Wu and Baeyens<sup>[23]</sup> and preliminary tests which have demonstrated that 20 min are enough for evidencing the effect on segregation of the studied variables. Once elapsed the selected fluidization time, the air supply was rapidly shut off, then the mixture was collected in six layers by a vacuum cleaner and sieved. Adsorbent and food materials were weighed separately to determine their concentration in each layer.

In the experiments performed in the L35b, the material vacuuming was started through a window with a removable plate located at the middle-height of a lateral wall and continued from the bed front by removing the Plexiglas window, while the vacuuming operation in the L20spjet was completely performed from the bed top. On the other hand, the settled bed surface was quite irregular turning difficult to measure an exact value for the bed height (and consequently, the value of  $h_{bed}/6$ ). Thus, although during the vacuum operation the layer thickness was maintained as regular as it was possible for all layers, it was not possible to take precise direct measure for it. Thus, the dimensionless thickness of layer  $i$  was estimated as:

$$\Delta h_i^* = \frac{\Delta h_i}{h_{bed}} = \frac{m_{Ai} + m_{Pi}}{m_A + m_P} \quad (6)$$

where  $m_A$  and  $m_P$  are the mass of adsorbent and product, respectively.

### Performed experiments and utilized nomenclature

Table 3 lists all the performed experiments in the L35b fluidized bed as well as in the spout-fluid bed (L20spjet), their ID, lyophilized material concentration, velocity, and air flow.

Based on the paper published by Donsi et al.,<sup>[18]</sup> the chosen concentrations for experiments were in terms of fresh product to adsorbent mass ratio, 1/20, 1/40, and 1/80.

Each experiment was identified with an alphanumeric code, such as *aaannnnRbbtee*, where *aaa* is the food material code (Table 1); *nnnn* is the theoretical  $u/u_{mfA}$  multiplied by 100; *bb* is the reciprocal of fresh product to adsorbent mass ratio (for lyophilized material, the corresponding mass ratio for the original fresh product is given); *ee* is the fluidization time in minutes.

**Table 3.** Conditions for performed experiments in the L35b fluidized bed and in the spout-fluid bed (identified by "L20spjet").

Experiment ID	Air flow (m <sup>3</sup> /h)	Material	$W_{PT}$	$u/u_{mfA}$
POd0260R40t20	210	Lyophilized potato	0.0046	2.75
POd0170R40t20	130	Lyophilized potato	0.0046	1.70
POd0150R40t20	120	Lyophilized potato	0.0046	1.54
POa0150R40t10	120	Lyophilized potato	0.0035	1.47
POa0150R80t10	120	Lyophilized potato	0.0016	1.47
POa0170R40t10	140	Lyophilized potato	0.0036	1.82
POa0170R80t10	140	Lyophilized potato	0.0017	1.71
PEb0260R20t20	200	Partially lyophilized pea	0.0138	2.57
PEb0170R80t20	140	Partially lyophilized pea	0.0039	1.75
PEa0260R20t20	200	Lyophilized pea	0.0093	2.57
PEa0260R80t20	200	Lyophilized pea	0.0023	2.56
PEc0230R20t20	175	Lyophilized pea	0.0109	2.42
PEc0190R20t20	145	Lyophilized pea	0.0109	1.93
PEa0150R20t20	120	Lyophilized pea	0.0089	1.49
PEa0150R80t20	120	Lyophilized pea	0.0024	1.49
CAa0260R20t20	200	Lyophilized carrot	0.0069	2.60
CAa0260R40t20	200	Lyophilized carrot	0.0033	2.60
CAa0260R80t20	200	Lyophilized carrot	0.0012	2.59
CAB0190R20t20	145	Lyophilized carrot	0.0053	1.85
CAa0170R20t20	140	Lyophilized carrot	0.0060	1.75
CAa0170R40t20	140	Lyophilized carrot	0.0032	1.76
CAa0170R80t20	140	Lyophilized carrot	0.0014	1.76
CAa0150R20t20	120	Lyophilized carrot	0.0067	1.50
CAa0150R40t20	120	Lyophilized carrot	0.0034	1.49
CAa0150R80t20	120	Lyophilized carrot	0.0013	1.50
CAB0150R20t40	120	Lyophilized carrot	0.0053	1.57
CAB0170R20t40	130	Lyophilized carrot	0.0053	1.66
CAB0260R20t40	200	Lyophilized carrot	0.0053	2.69
PEcR20L20spjet	37	Lyophilized pea	0.0109	0.51*
PEFR20L20spjet	37	Fresh pea	0.0500	0.51*
CABR20L20spjet	37	Lyophilized carrot	0.0053	0.51*
CAdR20L20spjet	37	Fresh carrot	0.0500	0.51*

\*Velocity of experiments performed in the L20spjet is not the relative air velocity  $u/u_{mfA}$ , but the absolute velocity,  $u$  (m/s).

## Results and discussion

### Nonfood wheat bran fluidization behavior

Unlike sand or other materials presenting formation of regular bubbles, wheat bran exhibits canalization or preferential air path formation, without regular generation of bubbles. Moreover, even if the air superficial velocity is augmented up to about twice the bran minimum fluidization velocity, the bed expansion remains at around minimum fluidization value and air "in excess" escapes through channels without rising the bed.

Considering the nonfood wheat bran PSD, its EDF and absolute density, this powder cannot be classified as cohesive (Geldart C). Nevertheless, it behaves like a Geldart C powder in a fluidized bed. This contradiction can be explained taking into account the physical characteristics of the bran particles such as rough surface and remains of grain brushes, leading to mechanical interactions (rather than electrostatic forces). Therefore, this kind of powder might be called "pseudo-cohesive."

As discussed in the Introduction, some works in the literature report changes in the fluidization behavior

due to variations in the moisture content of the fluidized material such as a shift in the Geldart behavior (from B or A type to A or A/C) and/or a reduction of the minimum fluidization velocity.<sup>[29 47–50]</sup> Nonetheless, taking into account the previous paragraphs, no significant effect of moisture content was assumed for nonfood wheat bran, as the channeling behavior would be merely accentuated in the worst case.

Furthermore, the existence of three zones along the bed (top, middle, and bottom) was observed in tests with the L20b fluidized bed. In the middle zone, there are no channels and air simply percolates through it, whereas at top and bottom the generation and collapse of channels follows a quite regular cyclical behavior. However, depending on air superficial velocity, the height of the middle zone can be very short (even null) or extend practically along all the fluidized bed. Despite these zones were observed only in the L20b fluidized bed, since its Plexiglas window completely covered one of its sides, their presence may be assumed for the L35b fluidized bed as well. Accordingly, segregation experiments using potato slabs (POd) have demonstrated the existence of these three zones as damaged potato slabs were found in the bed bottom due to the agitation in this part of the bed and their impossibility of rising the bed (see Segregation of binary mixtures for further information).

### Channel generation and collapse general cycle

Depending on air superficial velocity, only one big channel, few middle-sized channels, or very few small ones might form in the bed. In general terms, a cyclical behavior of channel generation and collapse can be observed (as described in Fig. 2). The number and shape of channels depend on air superficial velocity as well as on the position where they are formed in the bed.

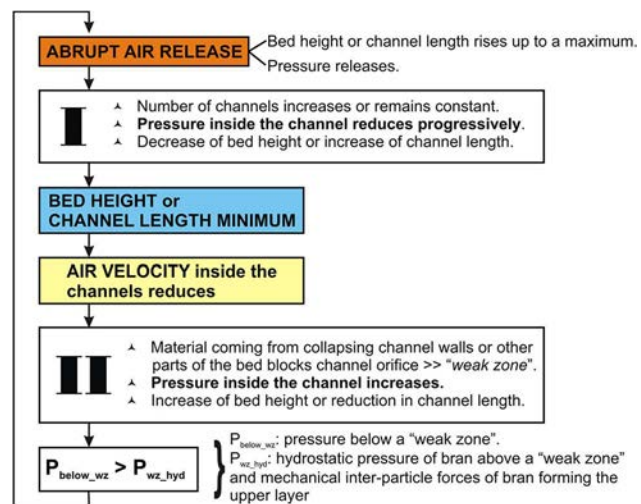


Figure 2. Channels generation (I) and collapse (II) general cycle.

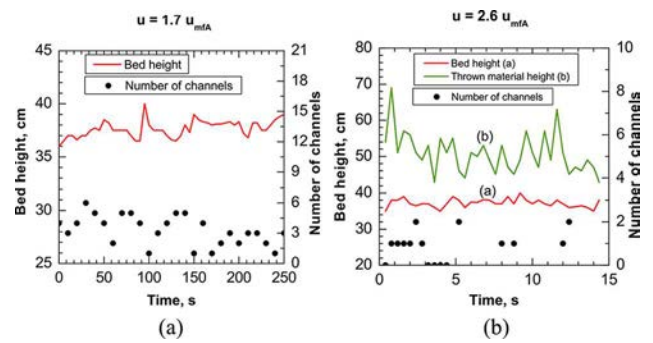


Figure 3. Number of channels and bed height at different air superficial velocities (in L35b fluidized bed). (a) Fluidization behavior at intermediate air velocity. (b) Fluidization behavior at high air velocity.

For example, by comparing the abscissas of Figs. 3a and 3b, it can be noted an increment on the oscillation frequency of bed height and channel generation and collapse as air superficial velocity is increased. In addition, a reduction of the average number of channels when increasing the mentioned variable can be observed. Hence, it can be said that this channeling behavior follows the general cycle shown in Fig. 2 represented with two main stages: I, generation and II, collapse.

Furthermore, from experimental observations, it can be said that the behavior of the channels generated in the upper part of the bed is comparable with that of a spouted bed (where three different regions, the annulus, the spout, and the fountain are present) whose air velocity is varied. In other words, it can be compared with the description given by Malek et al.<sup>[51]</sup> for the spout of a spouted bed as air velocity is raised. Therefore, the different phases of the channel generation and collapse general cycle are described as follows:

**Abrupt pressure release.** It may take place either near the bed surface, originating a path after a burst (Fig. 4,  $t=49.0$  s, square base 35-cm-sided fluidized bed, L35b) or far from the bed surface generating an internal channel extending up to a roof of compacted material. In the former case, the channel behaves like a spouted bed where air velocity has overcome the minimum spouting air velocity and a fountain of material thrown appears over the spout. Pressure drop through the channel reaches a maximum and starts decreasing and similarly occurs with air velocity inside the channel and fountain height reaching their maximum magnitudes. Inversely, bed height is minimum.

**Phase I (generation).** Pressure continues releasing, and new channels may appear as the result of the splitting of one single channel (Fig. 4, from  $t = 54.2$  s to  $t = 61.4$  s). Simultaneously, material coming from other parts of the



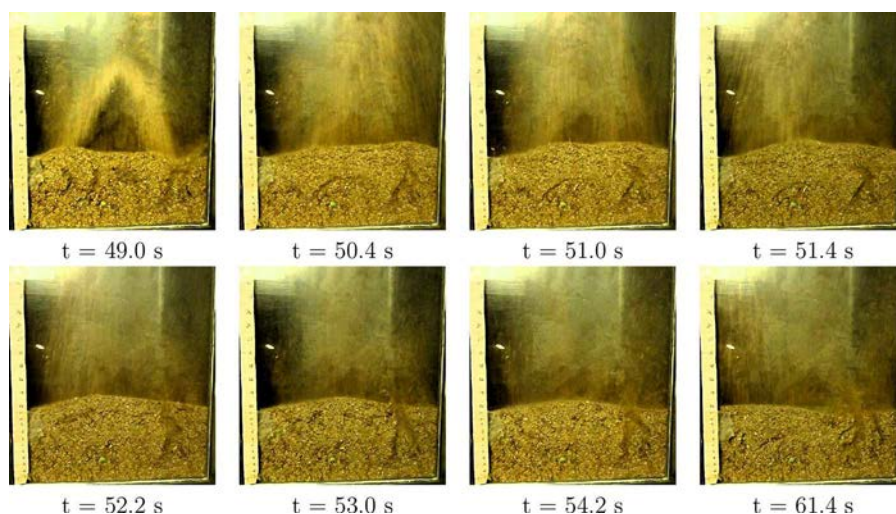


**Figure 4.** Generation, collapse, and generation of new channels (in L35b bed). On the right side of the fluidized bed, at a given  $t_0$  (49.0 s), and after a succession of other channel bursting (not shown in the figure), a new channel is generated, whose orifice starts to be covered by bran particles coming from other zones of the bed. After about 2 s ( $t=51.0$  s), the channel is blocked by bran particles creating a layer (“weak zone”). Under this layer pressure starts to increase, and a new burst is produced by the accumulated air, passing through a new path, increasing its velocity, and carrying up the material that previously formed the “weak zone” ( $t=52.2$  s). Thus, a new channel is generated, and since this explosion produces also the displacement and collapse of part of the adsorbent constituting the channel walls, the recently generated channel splits originating new channels ( $t=61.4$  s).

bed and/or collapsing channel walls starts blocking it until kinetic energy of coming out air is sufficient to drag the falling bran. If the channel is formed in the upper zone of the bed, a sudden decrease in fountain height can be seen. This situation is analogous to a spouted bed whose air velocity is progressively reduced after overcoming its minimum spouting velocity.

**Phase II (collapse).** Falling material blocks the channel orifice and air starts to be accumulated, increasing pressure below the material layer. When the pressure below the accumulated material is greater than the sum of the hydrostatic pressure caused by the plug and the forces embedding the material, a new abrupt air release takes place. In other words, the measured pressure drop continues reducing due to the increment

of pressure inside the channel (unlike it would be expected in a spouted bed whose pressure drop remains almost constant during air velocity reduction). In the case of upper channels, at the end of this phase, pressure drop as well as fountain height reach a minimum.

Thus, the layers above channels obstructing them constitute “weak zones” where the adsorbent is less compacted than the material in the surroundings. Nevertheless, not only the descending material in channel orifices can originate a “weak zone” but also the presence of another solid such as a food particle may induce it (Fig. 5, from  $t=91.8$  s to  $t=92.9$  s, square base 20-cm-sided fluidized bed, L20b).

More clear observations of the previously described cycle were done with experiments performed in the

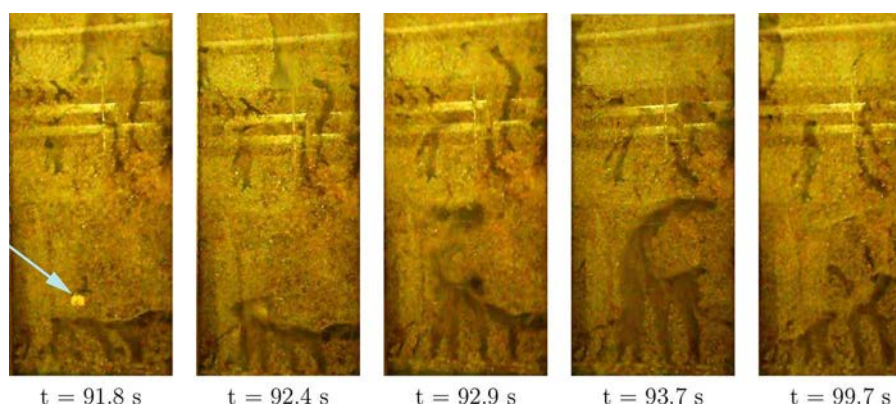


**Figure 5.** Generation of a channel from a “weak zone” induced by the presence of a piece of food material (at 92.4 s “weak zone” occurs). Observed near the bottom of the L20b bed.

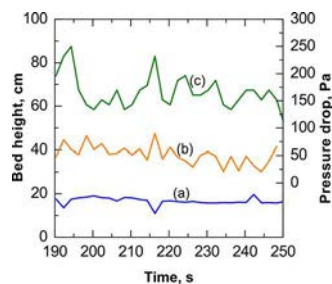


**Figure 6.** Oscillations of pressure drop (c), bed height (a), and height of thrown material (fountain) (b) during bran fluidization in the L065b bed; a 1-min representative snapshot is shown.

L065b bed (a snapshot of the most representative results is shown in Fig. 6). Due to the geometric characteristics of the bed (small diameter, cylindrical, etc) and bran particularities (such as mechanical interactions between particles), only one channel was formed, allowing the measurement of pressure drop and height of thrown material of a single channel without possible interferences caused by other channels.

Based on the fact that the standard deviation of the pressure drop varies practically linearly with the gas superficial air velocity (meaning that if the latter is 0, the former will be approximately 0 as well), several authors established a threshold for determining whether a defluidization process is taking place or not. This value can be estimated either by visual observations and/or other methods such as statistical or frequency domain analysis.<sup>[52–54]</sup>

In Fig. 7, the standard deviations of the variables shown in Fig. 6, estimated considering a moving time interval double of the average cycle time (calculated according to the criteria proposed by van Ommen et al.,<sup>[55]</sup>) are presented. In the present case, neither by visual observations, nor by analyzing the bed height and height of thrown material in Fig. 6, a defluidization

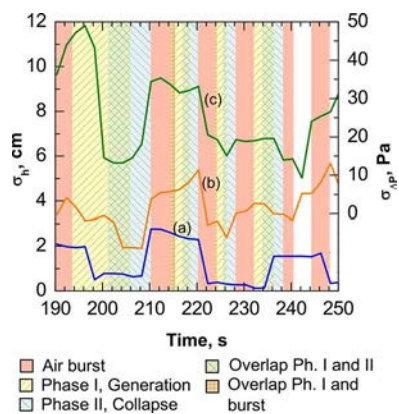


**Figure 7.** Standard deviations of the pressure drop (c), bed height (a), and height of thrown material (fountain) (b) presented in Fig. 6. The phases of the channel generation and collapse cycles are evidenced.

process can be detected. In addition, correlating the curve of the standard deviation of the pressure drop with those of the bed height and height of thrown material, it can be inferred that no defluidization occurs as their values are always larger than zero, meaning that bed material does not stop its movement. Therefore, no threshold can be established for defluidization.

On the other hand, the following observations can be made, evidencing the channel generation and collapse general cycle:

1. A sudden increment on the bed activity can be inferred from the increment of the standard deviations of the pressure drop and the thrown material in the “air burst” stage.
2. During Phase I of the cycle, the standard deviation of all measured variables reduces indicating a diminution of the air velocity inside the channel (which causes a simultaneous decrease in  $h_{bed}$  and  $\Delta P$ ).
3. In Phase II, the pressure drop is low while its standard deviation increases, which can be explained by an increase in the pressure inside the channel. Therefore, it can be said that the accumulated air inside the channel exerts a force on the upper bran particles which result in an increase in the bed height and the standard deviation of this variable.

On the other hand, analysis is much more complex in larger beds as several channels are simultaneously formed and generated at low air velocities, while the bed is chaotically agitated at high air velocities, but at least some qualitative agreements were found and the behavior can be inferred from the transport mechanisms of food particles hereafter described.

### Segregation of binary mixtures

In many works treating segregation and mixing, the concepts of *jetsam* (component tending to sink to the bed bottom) and *flotsam* (component tending to float to the bed top) introduced by Rowe et al.<sup>[21]</sup> are generally used. Nonetheless, as in the binary mixtures considered in the present work, the lighter component, the food product, is at the same time the larger one, it is not possible to establish a priori whether it will tend to sink or float. Hence, these terms will not be applied in the current discussion.

Figure 8a shows the segregation level as a function of the air superficial velocity to bran minimum fluidization velocity ratio for mixtures with partially and completely lyophilized material, whereas Fig. 8b represents the segregation level as a function of the equivalent fresh product to adsorbent mass ratio. In addition, in Table 4, the other TTSIS indices of these experiments are summarized.

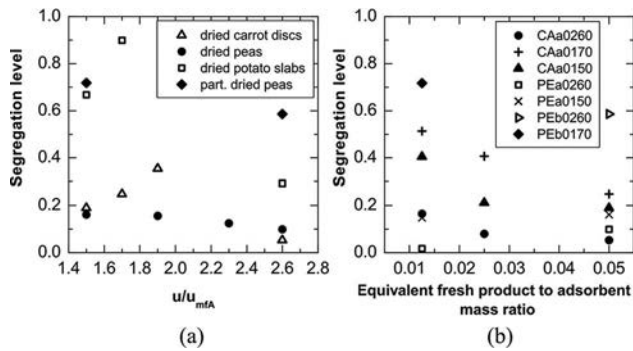


**Figure 8.** Effects of air superficial velocity and concentration on segregation in the L35b fluidized bed. (a) Segregation level as function of air superficial velocity relative to bran minimum fluidization velocity. Concentrations: R40 for dried potato slabs cases, R20 for the other ones. (b) Segregation level in terms of equivalent fresh product to adsorbent mass ratio (see Tables 1 and 3 for experiment and product code).

Results corresponding to experiments in the L35b with mixtures containing fresh food product are not presented neither in the figures nor in the tables since they exhibited full bottom segregation independently of air superficial velocity, product volume fraction, or food particle shape.

As it is seen in Fig. 8a, for dried carrot disks (CAa and CAb cases) and dried potato slabs (POd cases), the segregation level increases with air superficial velocity until a peak is reached (which can be assumed between 1.7 and  $\approx 2.4 u_{mfA}$ , depending on food material), and then it reduces to relatively low values at  $2.6 u_{mfA}$ . Similarly, in Fig. 8b, carrot (CAa) cases show the maximum segregation level at  $1.7 u_{mfA}$  (CAa0170) independently of product concentration. Nevertheless, lyophilized peas (PEa cases) present a completely different behavior; for this kind of binary mixtures, the segregation level is reduced almost linearly as air velocity increases.

About partially lyophilized peas, they have to be maintained in frozen state to conserve their structure. This fact makes this material difficult to handle. Anyway, two experimental points were acquired, and it was observed that very high segregation levels were obtained for these experiments, as a consequence of the higher density of the partially dried material in comparison with the dried one.

Besides, it is interesting to remark that segregation levels obtained using binary mixtures containing potato slabs (POd) are considerably greater than values obtained using mixtures with carrot disks (CAa, CAb), and values presented by mixtures containing peas (PEa, PEC) are notably lower than the other two binary mixtures. Therefore, since the difference in shape factor between carrot disks and peas is about 30%, and between potato slabs and peas is about 50%, it can be

**Table 4.** Results in terms of TTSIS for segregation experiments in the L35b with 20 min of fluidization time.

Experiment	$\rho_1$	$\rho_M$	$\rho_S$	$N_2$	Segregation type
POd0260R40t20	0.335	0.186	0.479	0.293	V-Top
POd0170R40t20	0.899	0.101	0.000	0.899	Bottom
POd0150R40t20	0.724	0.221	0.055	0.668	Bottom
POa0170R80t10	0.185	0.180	0.635	0.455	Top
POa0170R40t10	0.253	0.371	0.375	0.122	Top central
POa0150R80t10	0.000	0.011	0.989	0.989	Full top
POa0150R40t10	0.000	0.118	0.882	0.882	Top
PEb0260R20t20	0.715	0.155	0.129	0.586	Bottom
PEb0170R80t20	0.758	0.202	0.040	0.717	Bottom
PEa0260R80t20	0.322	0.339	0.339	0.017	Uniform
PEa0260R20t20	0.273	0.354	0.372	0.099	Top central
PEc0230R20t20	0.399	0.274	0.328	0.125	V-Bottom
PEc0190R20t20	0.411	0.255	0.334	0.156	V-Bottom
PEa0150R80t20	0.240	0.371	0.389	0.149	Top central
PEa0150R20t20	0.274	0.436	0.291	0.162	Central top
CAa0260R80t20	0.242	0.351	0.407	0.165	Top central
CAa0260R40t20	0.292	0.336	0.372	0.080	Top central
CAa0260R20t20	0.305	0.357	0.338	0.053	Uniform
CAb0190R20t20	0.544	0.265	0.191	0.354	Bottom central
CAa0170R80t20	0.612	0.289	0.099	0.513	Bottom
CAa0170R40t20	0.567	0.272	0.161	0.407	Bottom
CAa0170R20t20	0.299	0.475	0.226	0.249	Central bottom
CAa0150R80t20	0.091	0.496	0.413	0.405	Central top
CAa0150R40t20	0.206	0.377	0.417	0.212	Top central
CAa0150R20t20	0.240	0.430	0.330	0.190	Central top

TTSIS, three thirds segregation index set.

said that product sphericity plays a very important role on mixing of this kind of binary mixtures. What is more interesting to note is that, in experiments performed using POd, holey potato particles were found in the bed bottom, meaning that they descended but they could not ascend again due to their planar and wide shape. Consequently, potato pieces hit over the bed distributor screw causing their perforation.

Concerning segregation profiles, as it is seen in Tables 4 and 5, in general experiments at low and middle velocities ( $1.5\text{--}1.9 u_{mfA}$ ) exhibited intermediate behaviors of bottom segregation (bottom, bottom central, central bottom, and V-bottom). At high velocity ( $2.6 u_{mfA}$ ) nearly uniform profiles were obtained. In some cases at high velocity according to the classification criteria for segregation type, they are not uniform. However, not only the segregation type should be taken into account for evaluating the mixing but also the segregation level: despite the segregation profile was not uniform type, if the segregation level is low (approximately 0.15 or less), the distribution can be considered uniform to some extent.

**Table 5.** Results in terms of TTSIS for segregation experiments in the L35b with 40 min of fluidization time.

Experiment	$\rho_1$	$\rho_M$	$\rho_S$	$N_2$	Segregation type
CAb0150R20t40	0.682	0.228	0.090	0.591	Bottom
CAb0170R20t40	0.521	0.331	0.147	0.374	Bottom central
CAb0260R20t40	0.313	0.340	0.346	0.033	Uniform

TTSIS, three thirds segregation index set.

In mixtures containing partially lyophilized peas (PEb), a predominant bottom segregation and great segregation levels were found. Anyway, air velocity affects this last variable in the same way that in the other cases, reducing it.

Another experiment series where the influence of the air superficial velocity was highlighted is the one with lyophilized potato slabs (POa); particularly in the POa0170R40t10 case, starting with an induced top segregation, a nearly uniform segregation pattern was obtained after fluidizing the bed at high air superficial velocity. Also, the effect of product weight fraction on segregation is similar to CAa cases.

Regarding the effect of fluidization time, in Fig. 9a, it can be noted that as the time goes on the segregation profile changes from central top to bottom at  $1.5 u_{mfA}$  and from central bottom to bottom central at  $1.7 u_{mfA}$ , whereas at  $2.6 u_{mfA}$ , the segregation type is uniform independently of elapsed time. Considering the TTSIS of tracer particles in the figure, at  $1.5 u_{mfA}$ , it can be observed that particles initially in the bed bottom (iB) remained there, while food particles initially in the bed upper third (iT) moved toward bed bottom. A similar but less pronounced situation can be noted for cases at  $1.7 u_{mfA}$ . On the contrary, tracer particles at  $2.6 u_{mfA}$  are distributed more uniformly. Thus, two main conclusions can be drawn: first, product particle displacement toward bed bottom prevails at low velocities, and second, the peaks observed in the segregation level at intermediate velocities discussed in previous paragraphs may be only transient situations, prevailing the bottom segregation trend if fluidization time is increased.

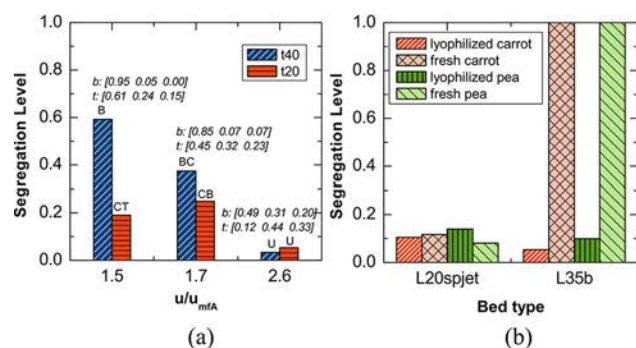


**Figure 9.** Fluidization time and performance of two different beds. (a) Effect of fluidization time on segregation as a function of relative air superficial velocity. Food material: lyophilized carrot disks (CAa, CAB). TTSIS for tracer particles corresponds to t40 experiments (b: initially in bottom, t: initially in top). (b) Performance of the fluidized bed (L35b) and the spout-fluid bed (L20spjet) for dried and fresh foodstuff. 20 min of fluidization time. Concentration: R20. Air superficial velocity in the L35b:  $2.6 u_{mfA}$ .

**Table 6.** Results in terms of TTSIS of tracer particles of segregation experiments presented in Tables 4, 5, and 7.

Experiment	Bottom tracers			Top tracers		
	$P_{IB}$	$P_{MB}$	$P_{SB}$	$P_{IT}$	$P_{MT}$	$P_{ST}$
CAb0190R20	0.822	0.072	0.106	0.221	0.464	0.315
POd0150R40	0.838	0.157	0.005			
POd0170R40	0.937	0.063	0.000	0.829	0.171	0.000
POd0260R40	0.402	0.176	0.422	0.079	0.209	0.712
PEc0190R20	0.000	0.000	1.000	0.393	0.324	0.283
PEc0230R20	0.518	0.204	0.278	0.240	0.292	0.467
CAb0150R20t40	0.950	0.050	0.000	0.609	0.238	0.152
CAb0170R20t40	0.852	0.074	0.074	0.448	0.320	0.232
CAb0260R20t40	0.488	0.315	0.196	0.118	0.444	0.438
PEcR20L20spjet	0.326	0.268	0.407	0.211	0.347	0.442
PEfR20L20spjet	0.339	0.393	0.268	0.263	0.362	0.375
CAdR20L20spjet	0.267	0.327	0.407	0.323	0.359	0.319
CAdR20L20spjet	0.564	0.228	0.208	0.309	0.311	0.379

TTSIS, three thirds segregation index set.

For example, in case CAb0190R20t20 (Table 6), it can be seen that while the most part of the bottom tracers remained in the bed bottom, a great part of the top tracers descended to the bed middle and bottom thirds. A more pronounced situation can be noted for POd0150R20t20 and POd0170R20t20 cases, where practically all the bottom tracer remained in the bed bottom, and the greatest part of the top tracer particles was found in the lowest third of the bed.

On the other hand, a different distribution of the tracer particles can be observed for PEc cases, which are more uniformly distributed than tracers of CAb and POd. That would mean that the V-type of segregation profiles presented by mixtures containing this material might be also a transient stage. Thus, it might be asseverated that they may evolve to uniform profiles as time goes on.

From experiments utilizing six binary mixtures combining materials with different properties (density, size, and minimum fluidization velocity) in a two-dimensional fluidized bed, Rowe et al.<sup>[21]</sup> found four main segregation mechanisms, valid for bubbling fluidized beds. These mechanisms are based on the interaction of the materials with the bubbles (lifting in the bubbles wakes, or falling of denser and larger particles through their free space), and particle interactions (interparticle percolation of smaller and denser particles through large and light ones, and quasi-hydrostatic effect, when lighter particles float on a bed of denser particles).

Unlike the cases where a binary mixture is fluidized in a bubbling fluidized bed and bubbles are the main mixing agent, in channeling fluidized bed the mixing might be attributed mainly to the shaking of the bed, and channels generation and collapse cycles. Thus, three main types of product particle movement mechanisms can be individuated: passive transport (downward), active transport (upward), and movement blocking,

which only in part may be analogous or similar in some way to those described by Rowe. Moreover, the presence and frequency of these mechanisms depend upon air superficial velocity, and they often occur simultaneously in different parts of the bed.

In passive transport (Fig. 10), adsorbent material below food particles is dragged by air through channel orifices and deposited on bed surface. Consequently, a downward motion of foodstuff takes place as a result of the collapse of the generated void under it. On the opposite, a food particle is actively transported when it is dragged by air and other bran particles through the channels in upward direction (see Fig. 11; this mechanism may correspond to lifting of particles enclosed in rising bubble wakes which occurs in bubbling fluidized beds).

Additionally, as a result of interaction between adsorbent particles, two main effects causing particle blocking may be identified: floor effect and roof effect (Fig. 10,  $t_3$ ). The former is caused by agglomerates of embedded bran particles or more compacted zones avoiding the fall of product particles. The compaction level decreases increasing air superficial velocity mainly because of a higher mobility in the fluidized bed. The latter blocking effect occurs when either a food particle is covered by adsorbent due to the collapse of a channel wall (Fig. 10,  $t_3$ ), or a layer of more compacted material is present above it, obstructing the possibility of ascendant movement. These effects may be considered the correspondent ones to the quasi-hydrostatic effects described by Rowe et al.<sup>[21]</sup> but are completely different in their causes.

At high velocities ( $2.3\text{--}2.6 u_{mfA}$ ,  $0.39\text{--}0.44$  m/s) pressure release takes place through only one channel of large diameter. In each air burst, a fountain reaching fountain

heights of about twice the bed height is generated (as it was presented in Fig. 3). The channel generation and collapse cycle repeat at elevated frequencies, and food particles are actively transported by air and moving bran particles. At the same time, due to bed agitation, floor effect is practically absent allowing passive transport during channel collapse. Consequently, the lyophilized material uniformly distributes along the bed.

At intermediate velocities ( $1.7\text{--}1.9 u_{mfA}$ ,  $0.29\text{--}0.32$  m/s), the number of channels often increases after a burst by splitting the original one. Although air velocity inside them seems to be not sufficient for continuously dragging food material. Furthermore, due to the vibration of bran particles, the floor effect is quite reduced and food particles sink. Moreover, during the second stage of the cycle, pressure has been completely released and the number of channels reduces due to collapse of their walls and material depositing over them. Thus, even if a channel was generated at bed bottom, food particles could not ascend due to roof effect. In particular, as it was previously said, in POd cases, perforated potato particles were found in the bed bottom, where evidently particles are agitated and hit the distributor screw. More specifically, case POd0170R40 presented the maximum quantity of damaged food particles (about 44%) among all experiments using POd.

At low velocity ( $1.5 u_{mfA}$ ,  $0.25$  m/s), one or two small diameter channels are detected. A complete absence of channels in the second stage of the channel generation and collapse cycle is also possible. As a consequence of this practically lack of shaking, floor and roof effects are notably high avoiding food particles' sinking and eventual ascendant movements. Therefore, passive transport

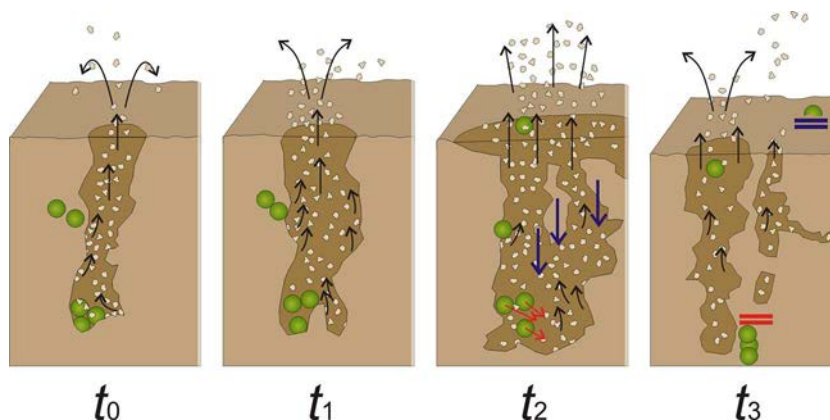


**Figure 10.** Passive transport and blocking effects, during the generation (or expansion) and collapse of a channel. Bran is dragged by air from channel walls producing cavities under food particles ( $t_0$ ), and leading to their displacement ( $t_1$ ). After an air burst, some food particles move toward the new generated space ( $t_2$ , red arrows), and simultaneously, bran from the collapsing channel walls covers the recently deposited food particles (blue arrows). Finally, food particles in the channel bottom are completely covered by bran and their upwards movement is blocked by roof effect ( $t_3$ ). In addition, the downward movement of a deposited particle on the bed surface is blocked by floor effect. Also some particles may be actively transported during the channel generation-collapse process ( $t_2$  and  $t_3$ ).

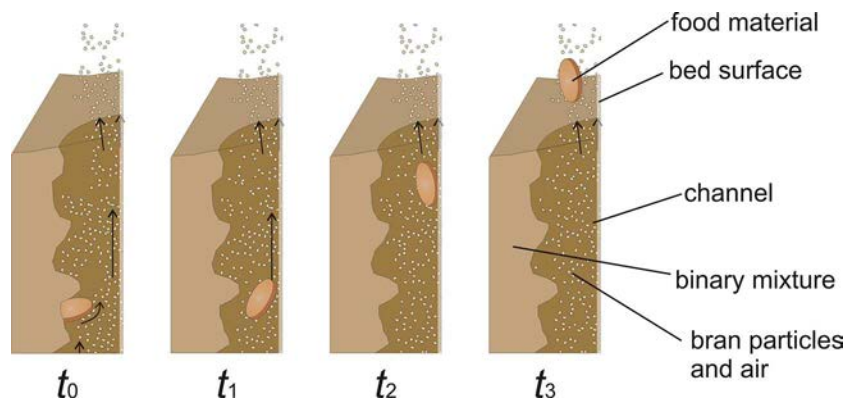


**Figure 11.** Active transport of a food particle. At  $t_0$  bran particles are dragged by air, impacting on the greater particle surface and transferring their momentum. Then, the food particle is moved from its embedded position and dragged by air.

prevails causing the foodstuff movement toward bed bottom and the effect of particle shape and size is highlighted. In fact, wide and planar shaped particles (like POd) descend by passive transport, but they can not ascend again in part because of roof effect, and in part due to the fact that particles are not able to enter into channels of small diameter. On the other hand, disks or spherical particles can be eventually actively transported when a channel is generated. Anyway, as it was demonstrated in experiments with 40 min of fluidization time ( $t_{40}$  cases), the downward movement prevails as time goes on.

With regard to the effect of food volumetric fraction, no general regular pattern can be observed for all the analyzed cases. For lyophilized carrots and potatoes (CAa and POa cases), a decrement of the segregation level is observed increasing food product volumetric fraction, while with peas (PEa cases) that parameter increases with food material concentration. At high velocity, a possible explanation might be formulated taking into account the number of “weak zones” induced by the bigger solid and its shape. In the case of disks, for example, increasing foodstuff concentration, the number of “weak zones” increases, resulting in a greater number of channels. In addition, the planar shape and relatively small size might lead to a lower compaction of the material, and thus, passive transport globally compensates active transport resulting in a uniform mixing. On the opposite, spherical particles are actively transported easier than planar ones causing lower segregation levels than disks (as shown in Fig. 8b). Thus, the greater concentration, the bigger

number of “weak zones,” and more foodstuff particles are actively transported inside the channels.

Finally, Fig. 9b shows a comparison between the L35b (fluidized bed) and the L20spjet (fluid-spout bed). It can be noted that while in the L35b the binary mixture is completely segregated for fresh product, the segregation level obtained in experiments performed in the L20spjet is considerably low (below 0.15) for all tested food materials. Moreover, TTSIS results of experiments performed in the L20spjet (Table 7) exhibit a quite uniform distribution. Furthermore, in Table 6, it is possible to see that in L20spjet experiments, tracer particles (both initially bottom and initially top tracers) exhibit uniform distributions in all the considered cases. These results evidence that food material is continuously distributed all along the bed during fluidization.

From the point of view of the previously mentioned transport mechanisms, the outcomes of experiments in the fluid-spout bed can be explained as follows. In the L20spjet, only a central channel generated by the bed main injector is present, and its walls are constituted by compacted bran deposited by the fountain. Thus, food particles and adsorbent are transported actively in the central channel to bed surface and passively in downward direction by bran in the annulus. Lateral air injectors avoid product concentration in bed bottom pushing it to the central channel, allowing an accurate mixing of the binary mixture.

## Conclusion

In AFD, by IAM performed in fluidized or spout-fluid bed, a good contact between the food material and the adsorbent is important to avoid the air saturation, taking advantage of the heat of adsorption for sublimating ice. Nonfood wheat bran is a very promising material to be used as adsorbent. However, despite the fact that according to its population size distribution and EDF, it would be classified as a Geldart B powder,

**Table 7.** Results in terms of TTSIS for segregation experiments in the L20spjet with 20 min of fluidization time.

Experiment	$\rho_l$	$\rho_M$	$\rho_s$	$N_2$	Segregation type
PEcR20L20spjet	0.265	0.330	0.405	0.140	Top central
PEfR20L20spjet	0.292	0.373	0.334	0.081	Central top
CAdR20L20spjet	0.272	0.339	0.389	0.117	Top central
CAbR20L20spjet	0.403	0.298	0.299	0.105	V-Bottom

TTSIS, three thirds segregation index set.

it fluidizes like a Geldart C. Thus, it can be considered a “pseudo-cohesive” powder. This behavior may lead to potential difficulties in handling the binary mixture when the AFD process is performed in a fluidized bed.

In addition, as it was expected from the theory, it was evidenced that, even for a binary mixture composed by a pseudo-cohesive powder and a solid whose particles are considerably greater than the powder ones, the air superficial velocity plays a very important role in mixing. Particularly, at high air flows ( $2.6 u_{mfA}$  for the analyzed cases) uniform distribution of the material of interest is reached when dried foodstuff is used. Nonetheless, product density plays a fundamental role, since nonuniform segregation profiles were obtained when fresh or partially lyophilized food material was considered, resulting in a poor contact between adsorbent and food material in the first stages of the AFD process in a fluidized bed.

Two food particle transport mechanisms (passive and active) and two movement blocking effects (floor and roof effects) were proposed to explain the observed behaviors. This, together with the channel generation and collapse cycle, permitted to explain the segregation phenomenon in channeling fluidized beds and the mixing process in fluid-spout beds.

Uniform mixing profiles were reached in the fluid-spout bed with a good circulation of the food particles along the bed during fluidization. These results showed to be independent of the product density. Thus, this kind of bed should be used if an uniform mixing between adsorbent and food product is desired in the process of AFD with use of adsorbent.

## Acknowledgments

The present work was based on the PhD thesis of the corresponding author. In addition, the authors wish to thank Massimo Curti and Giorgio Rovero for their practical help and recommendations in the fluidization field and equipment operation.

## Funding

The EUROTANGO Project (from the Erasmus Mundus Programme) is acknowledged for funding Mauricio M. Coletto's PhD studies.

## Nomenclature

$d$	food particle diameter	mm
$d_{eq}$	equivalent diameter for fluidization	m
$d_{SV}$	Sauter's diameter	mm
$F_q$	accumulated mass of material of interest “q” from the bottom	kg

$g$	gravity acceleration	m/s <sup>2</sup>
$h^*$	dimensionless position in the bed from the bottom	-
$h_{bed}$	total bed height in settled state	m
$\Delta h_i$	layer $i$ thickness	m
$\Delta h_i^*$	dimensionless thickness of layer	-
$l, l_1, l_2, l_3$	food particle lengths	mm
$m$	mass	kg
$\Delta P$	pressure drop	Pa
$p_I$	bottom third indicator, in TTSIS (Eq. 2)	-
$p_M$	middle third indicator, in TTSIS (Eq. 3)	-
$p_S$	top third indicator, in TTSIS (Eq. 4)	-
$t, t_0$	time, and reference starting time	s
$u$	air superficial velocity	m/s
$u_{mf}$	minimum fluidization velocity	m/s
$w_{PT}$	overall food product mass fraction	-

### Greek letters

$\mu$	air viscosity	Pa s
$\rho$	density	kg/m <sup>3</sup>
$\sigma_{\Delta P}$	standard deviation of the pressure drop	Pa
$\sigma_h$	standard deviation of the bed height	cm
$\psi$	particle shape factor	-

### Others

$\aleph_2$	segregation level	-
------------	-------------------	---




### Subscripts

A	adsorbent (nonfood wheat bran)	
air	air	
$b$	tracer particles initially in bed bottom	-
$i$	layer $i$	
P	food product	
q	material of interest “q”	
T	total	
$t$	tracer particles initially in bed top	-

### Acronyms

AFD	atmospheric freeze drying
EDF	equivalent diameter for fluidization
FB	fluidized bed
IAM	immersion in an adsorbent medium
PSD	particle size distribution
TTSIS	three thirds segregation index set
VFD	vacuum freeze drying

## ORCID

Mauricio M. Coletto  <http://orcid.org/0000-0003-0523-5282>  
 Daniele L. Marchisio  <http://orcid.org/0000-0002-9104-0571>  
 Antonello A. Barresi  <http://orcid.org/0000-0002-9104-0571>

## References

- [1] Claussen, I.; Ustad, T.; Strømmen, I.; Walde, P. Atmospheric freeze drying - A review. *Drying Technology* **2007**, *25*(6), 947–957.
- [2] Fissore, D.; Velardi, S. Freeze drying: Basic concepts and general calculation procedures. In *Operations in Food Refrigeration*; Mascheroni, R., Ed.; CRC Press: Boca Raton, FL, 2012; Chapter 3, 47–70.
- [3] Barresi, A.; Fissore, D. Freeze-drying equipments. In *Operations in Food Refrigeration*; Mascheroni, R., Ed.; CRC Press - Taylor & Francis Group (CAN), 2012; Chapter 18, 353–369.
- [4] Eikevik, T.M.; Alves-Filho, O.; Bantle, M. Microwave-assisted atmospheric freeze drying of green peas: A case of study. *Drying Technology* **2012**, *30*, 1592–1599.
- [5] Zielinska, M.; Zapotoczny, P.; Alves-Filho, O.; Eikevik, T.M.; Blaszcak, W. Microwave vacuum-assisted drying of green peas using heat pump and fluidized bed: A comparative study between atmospheric freeze drying and hot air convective drying. *Drying Technology* **2013**, *31*(6), 633–642.
- [6] Bantle, M.; Eikevik, T.M. Parametric study of high-intensity ultrasound in the atmospheric freeze drying of peas. *Drying Technology* **2011**, *29*, 1230–1239.
- [7] Santacatalina, J.; Fissore, D.; Cárcel, J.; Mulet, A.; García-Pérez, J. Model-based investigation into atmospheric freeze drying assisted by power ultrasound. *Journal of Food Engineering* **2015**, *151*, 7–15.
- [8] Pisano, R.; Fissore, D.; Barresi, A. Intensification of freeze-drying for the pharmaceutical and food industry. In *Modern Drying Technology Vol. 5: Process Intensification*; Tsotsas, E., Mujumdar, A.S., Eds.; Wiley-VCH Verlag GmbH & Co. KGaA: Weinheim, 2014; Chapter 5, 131–161.
- [9] Donsì, G.; Ferrari, G.; Di Matteo, P. Utilization of combined processes in freeze-drying of shrimps. *Food and Bioproducts Processing, Transactions of the Institution of Chemical Engineers, Part C* **2001**, *79*(3), 152–159.
- [10] Bustos, R.; Vásquez, M.; Vega, R.; Reyes, A.; Bubnovich, V.; Scheuermann, E. Comparative study of different process conditions of freeze drying of “murtilla” berry. *Drying Technology* **2010**, *28*, 1416–1425.
- [11] Boeh-Ocansey, O. Some factors influencing the freeze drying of carrot discs in vacuo and at atmospheric pressure. *Journal of Food Engineering* **1985**, *4*, 229–243.
- [12] Reyes, A.; Mahn, A.; Huenulaf, P. Drying of apple slices in atmospheric and vacuum freeze dryer. *Drying Technology* **2011**, *29*, 1076–1089.
- [13] Claussen, I.; Strømmen, I.; Hemmingsen, A.T.; Rustad, T. Relationship of product structure, sorption characteristics, and freezing point of atmospheric freeze-dried foods. *Drying Technology* **2007**, *25*, 853–865.
- [14] Claussen, I.; Anssessen, T.; Eikevik, T.; Strømmen, I. Atmospheric freeze drying - Modeling and simulation of a tunnel dryer. *Drying Technology* **2007**, *25*, 1959–1965.
- [15] Rahman, S.; Mujumdar, A. A novel atmospheric freeze drying system using a vibro-fluidized bed with adsorbent. *Drying Technology* **2008**, *26*, 393–403.
- [16] Reyes, A.; Vega, R.V.; Bruna, R.D. Effect of operating conditions in atmospheric freeze drying of carrot particles in a pulsed fluidized bed. *Drying Technology* **2010**, *28*(10), 1185–1192.
- [17] Duan, X.; Yang, X.; Ren, G.; Pang, Y.; Liu, L.; Liu, Y. Technical aspects in freeze-drying of foods. *Drying Technology* **2016**, *34*(11), 1271–1285.
- [18] Donsì, G.; Di Matteo, P.; Ferrari, G. The role of heat and mass transfer phenomena in atmospheric freeze-drying of foods in a fluidised bed. *Journal of Food Engineering* **2003**, *59*, 267–275.
- [19] Di Matteo, P. *Sviluppo di un processo per la liofilizzazione a pressione atmosferica di sostanze alimentari*. Ph.D. thesis. Università degli Studi di Salerno, **2002**.
- [20] Wolff, E.; Gibert, H. Atmospheric freeze-drying part 2: Modeling drying kinetics using adsorption isotherms. *Drying Technology* **1990**, *2*(8), 405–428.
- [21] Rowe, P.; Nienow, A.; Agbim, A. The mechanisms by which particles segregate in gas fluidised beds - binary systems of near-spherical particles. *Transactions of the Institution of Chemical Engineers* **1972**, *50*(4), 310–323.
- [22] Qiaoquna, S.; Huilina, L.; Wentiea, L.; Yuronga, H.; Lidana, Y.; Gidaspow, D. Simulation and experiment of segregating/mixing of rice husk-sand mixture in a bubbling fluidized bed. *Fuel* **2005**, *84*, 1739–1748.
- [23] Wu, S.; Baeyens, J. Segregation by size difference in gas fluidized beds. *Powder Technology* **1998**, *98*, 139–150.
- [24] Chew, J.; Hrenya, C. Link between bubbling and segregation patterns in gas-fluidized beds with continuous size distributions. *AIChE Journal* **2011**, *57*(11), 3003–3011.
- [25] Geldart, D. Types of gas fluidization. *Powder Technology* **1973**, *7*, 285–292.
- [26] Bi, H.T. A critical review of the complex pressure fluctuation phenomenon in gas–solids fluidized beds. *Chemical Engineering Science* **2007**, *62*(13), 3473–3493.
- [27] Visser, J. van der Waals and other cohesive forces affecting powder fluidization. *Powder Technology* **1989**, *1*, 1–10.
- [28] Geldart, D.; Harnby, N.; Wong, A. Fluidization of cohesive powders. *Powder Technology* **1984**, *31*(1), 25–37.
- [29] Wright, P.; Raper, J. Role of liquid bridge forces in cohesive fluidization. *Transactions of the Institution of Chemical Engineers, Part A* **1998**, *76*, 753–760.
- [30] Sundaresan, S. Instabilities in fluidized beds. *Annual Review of Fluid Mechanics* **2003**, *35*, 63–88.
- [31] Zhou, T.; Li, H. Estimation of agglomerate size for cohesive particles during fluidization. *Powder Technology* **1999**, *101*, 57–62.
- [32] van Wachem, B.; Sasic, S. Derivation, simulation and validation of a cohesive particle flow CFD model. *AIChE Journal* **2008**, *54*(1), 9–19.
- [33] Sutanto, W. *Hydrodynamics of spout fluid beds*. Ph.D. thesis. University of British Columbia, 1981.
- [34] Zhang, Y.; Zhong, W.; Jin, B.; Xiao, R. Mixing and segregation behavior in a spout-fluid bed: Effect of particle size. *Industrial and Engineering Chemistry Research* **2012**, *51*, 14247–14257.
- [35] Du, W.; Zhang, L.; Zhang, B.; Bao, S.; Xu, J.; Wie, W. Pressure drop and pressure fluctuations in spouted beds



- with binary mixtures of particles. *Powder Technology* **2015**, *276*, 134–143.
- [36] Kumar, B.S.; Vinod, A.V. Mixing characteristics of binary mixtures in a spout-fluid bed. *Particulate Science and Technology* **2016**, In press. doi:10.1080/02726351.2016.1146810.
- [37] Zhang, Y.; Zhong, W.; Jin, B.; Xiao, R. Mixing and segregation behavior in a spout-fluid bed: Effect of particle density. *Industrial and Engineering Chemistry Research* **2013**, *52*, 5489–5497.
- [38] Passos, M.L.; Mujumdar, A.S.; Vijaya, G.; Raghavan, V.G. Spouted and spout-fluidized beds for gram drying. *Drying Technology* **1989**, *7*(4), 663–696.
- [39] Lima, A.C.C.; Rocha, S.C.S. Bean drying in fixed, spouted and spout-fluid beds: A comparison and empirical modeling. *Drying Technology* **1998**, *16*(9–10), 1881–1901.
- [40] Zhong, W.; Chen, X.; Zhang, M. Hydrodynamic characteristics of spout-fluid bed: Pressure drop and minimum spouting/spout-fluidizing velocity. *Chemical Engineering Journal* **2006**, *118*(1–2), 37–46.
- [41] Link, J.; Cuypers, L.; Deen, N.; Kuipers, J. Flow regimes in a spout-fluid bed: A combined experimental and simulation study. *Chemical Engineering Science* **2005**, *60*(13), 3425–3442.
- [42] Zhang, J.; Tang, F. Prediction of flow regimes in spout-fluidized beds. *China Particology* **2006**, *4*(3–4), 189–193.
- [43] Zhong, W.; Zhang, M.; Jin, B.; Yuan, Z. Three-dimensional simulation of gas/solid flow in spout-fluid beds with kinetic theory of granular flow. *Chinese Journal of Chemical Engineering* **2006**, *14*(5), 611–617.
- [44] Wang, S.; Zhao, L.; Wang, C.; Liu, Y.; Gao, J.; Liu, Y.; Cheng, Q. Numerical simulation of gas–solid flow with two fluid model in a spouted-fluid bed. *Particology* **2014**, *14*, 109–116.
- [45] Coletto, M. *Atmospheric freeze drying of food in fluidized beds - Practical aspects and CFD simulation*. Ph.D. thesis. Politecnico di Torino, 2015. doi:10.6092/polito/porto/2588248.
- [46] Coletto, M.; Marchisio, D.; Barresi, A. A new segregation index for solid multicomponent mixtures. *Powder Technology* **2016**, *299*, 77–86.
- [47] Wormsbecker, M.; Pugsley, T. The influence of moisture on the fluidization behaviour of porous pharmaceutical granule. *Chemical Engineering Science* **2008**, *63*, 4063–4069.
- [48] Zhou, H.; Xiong, Y.; Pei, Y. Effect of moisture content on dense-phase pneumatic conveying of pulverized lignite under high pressure. *Powder Technology* **2016**, *287*, 355–363.
- [49] Makkawi, Y.; Wright, P. Tomographic analysis of dry and semi-wet bed fluidization: The effect of small liquid loading and particle size on the bubbling behaviour. *Chemical Engineering Science* **2004**, *59*, 201–213.
- [50] McLaughlin, L.; Rhodes, M. Prediction of fluidized bed behaviour in the presence of liquid bridges. *Powder Technology* **2001**, *114*, 213–223.
- [51] Malek, M.; Benjamin, C.; Lu, Y. Pressure drop and spoutable bed height in spouted beds. *I&EC Process Design and Development* **1965**, *4*(1), 123–128.
- [52] van Ommen, J.; de Corte, R.; van den Bleek, C. Rapid detection of defluidization using the standard deviation of pressure fluctuations. *Chemical Engineering and Processing* **2004**, *43*, 1329–1335.
- [53] Gómez-Hernández, J.; Soria-Verdugo, A.; Villa Briongos, J.; Santana, D. Fluidized bed with a rotating distributor operated under defluidization conditions. *Chemical Engineering Journal* **2012**, *195–196*, 198–207.
- [54] Serrano, D.; Sánchez-Delgado, S.; Sobrino, C.; Marugán-Cruz, C. Defluidization and agglomeration of a fluidized bed reactor during *Cynara cardunculus* L. gasification using sepiolite as a bed material. *Fuel Processing Technology* **2015**, *131*, 331–347.
- [55] van Ommen, J.; Srdjan, S.; van der Schaaf, J.; Gheorghiu, S.; Johnsson, F.; Marc-Olivier, C. Time-series analysis of pressure fluctuations in gas-solid fluidized beds - A review. *International Journal of Multiphase Flow* **2011**, *37*, 403–428.